Structure and stability of recombinant bovine odorant-binding protein: II. Unfolding of the monomeric forms

Olga V Stepanenko, Denis O Roginskii, Olesya V Stepanenko, Irina M Kuznetsova, Vladimir N Uversky, Konstantin K Turoverov

In a family of monomeric odorant-binding proteins (OBPs), bovine OBP (bOBP), that lacks conserved disulfide bond found in other OBPs, occupies unique niche because of its ability to form domain-swapped dimers. In this study, we analyzed conformational stabilities of the recombinant bOBP and its monomeric variants, the bOBP-Gly121+ mutant containing an additional glycine residue after the residue 121 of the bOBP, and the GCC-bOBP mutant obtained from the bOBP-Gly121+ form by introduction of the Trp64Cys/His155Cys double mutation to restore the canonical disulfide bond. We also analyzed the effect of the natural ligand binding on the conformational stabilities of these bOBP variants. Our data are consistent with the conclusion that the unfolding-refolding pathways of the recombinant bOBP and its mutant monomeric forms bOBP-Gly121+ and GCC-bOBP are similar and do not depend on the oligomeric status of the protein. This clearly shows that the information on the unfolding-refolding mechanism is encoded in the structure of the bOBP monomers. However, the process of the bOBP unfolding is significantly complicated by the formation of the domain-swapped dimer, and the rates of the unfolding-refolding reactions essentially depend on the conditions in which the protein is located.

Structure and Stability of Recombinant Bovine Odorant-Binding Protein: II. Unfolding of the Monomeric Forms

Olga V. Stepanenko,[1] Denis O. Roginskii,[1] Olesya V. Stepanenko,[1] Irina M. Kuznetsova,[1] Vladimir N. Uversky,[1,2,*] and Konstantin K. Turoverov[1,3,*]

[1]*Laboratory of structural dynamics, stability and folding of proteins, Institute of Cytology, Russian Academy of Sciences, St. Petersburg, Russia;*

[2]*Department of Molecular Medicine and USF Health Byrd Alzheimer's Research Institute, Morsani College of Medicine, University of South Florida, Tampa, FL, USA;*

[3]*Peter the Great St. Petersburg Polytechnic University, St. Petersburg, Russia*

***To whom correspondence should be addressed**: VNU, Department of Molecular Medicine, University of South Florida, 12901 Bruce B. Downs Blvd. MDC07, Tampa, Florida 33612, USA, E-mail: vuversky@health.usf.edu; KKT, Institute of Cytology, Russian Academy of Sciences, Tikhoretsky Av., 4, St. Petersburg 194064, Russia, E-mail: kkt@incras.ru

Running title: Unfolding of the monomeric bOBP variants

ABSTRACT

In a family of monomeric odorant-binding proteins (OBPs), bovine OBP (bOBP), that lacks conserved disulfide bond found in other OBPs, occupies unique niche because of its ability to form domain-swapped dimers. In this study, we analyzed conformational stabilities of the recombinant bOBP and its monomeric variants, the bOBP-Gly121+ mutant containing an additional glycine residue after the residue 121 of the bOBP, and the GCC-bOBP mutant obtained from the bOBP-Gly121+ form by introduction of the Trp64Cys/His155Cys double mutation to restore the canonical disulfide bond. We also analyzed the effect of the natural ligand binding on the conformational stabilities of these bOBP variants. Our data are consistent with the conclusion that the unfolding-refolding pathways of the recombinant bOBP and its mutant monomeric forms bOBP-Gly121+ and GCC-bOBP are similar and do not depend on the oligomeric status of the protein. This clearly shows that the information on the unfolding-refolding mechanism is encoded in the structure of the bOBP monomers. However, the process of the bOBP unfolding is significantly complicated by the formation of the domain-swapped dimer, and the rates of the unfolding-refolding reactions essentially depend on the conditions in which the protein is located.

Key words: odorant-binding protein; domain swapping; disulfide bond; unfolding-refolding reaction; ligand binding; conformational stability

INTRODUCTION

Odorant binding proteins (OBPs) are important components of olfactory apparatus in vertebrates where they play a specific role in olfaction by interacting directly with odorants (Xu et al. 2005). OBPs constitute a class of small extracellular proteins in the chemosensory systems of most terrestrial species ranging from drosophila to human. In mammals, OBPs are found at high concentrations (~10 mM) in nasal mucosa of cow (Bignetti et al. 1985; Pelosi et al. 1982), rat (Pevsner et al. 1985), rabbit (Dal Monte et al. 1991), pig (Dal Monte et al. 1991), dog (D'Auria et al. 2006), and humans (Briand et al. 2002). Although they bind different kinds of small and hydrophobic odorant molecules (typically with the affinities in the micromolar range, their inability to discriminate different chemical classes of these molecules suggests that OBPs cannot serve as olfactory receptors (Boudjelal et al. 1996). The precise biological functions of mammalian OBPs are not known as of yet, but it was hypothesized that these proteins can be involved in transport of hydrophobic odorants across the aqueous mucus layer to access the olfactory receptors, or might be involved in the termination of the olfactory signal by removing odorants from the receptors after their stimulation (Bignetti et al. 1987; Pevsner & Snyder 1990).

OBPs constitute a sub-class of lipocalins, which are small extracellular proteins found in gram negative bacteria, plants, invertebrates, and vertebrates. Although lipocalins are known to share limited regions of sequence homology, they do have a common tertiary structure architecture (Flower et al. 2000; Grzyb et al. 2006). The characteristic structural signature of the lipocalin family is a β-barrel composed by a 9-stranded anti-parallel β-sheet with an α-helical segment at the C-terminus (Flower et al. 2000). The internal cavity of the lipocalin β-barrel is the binding site that can interact with the odorant molecules belonging

65 to different chemical classes (Vincent et al. 2000). Bovine OBP (bOBP) was the first OBP
66 for which crystal structure was solved, and the analysis of this structure revealed that bOBP
67 exists as a domain-swapped dimer (Bianchet et al. 1996; Tegoni et al. 1996). This was in
68 contrast to structures of other lipocalins, including the porcine OBP (pOBP) (Spinelli et al.
69 1998), which are monomeric proteins. The ability of bOBP to form domain-swapped dimers
70 was explained by the absence of a glycine residue at the hinge region linking the β-barrel to
71 the α–helix, and by the lack of the disulfide bridge which is present in all lipocalin sequences
72 identified so far (Ramoni et al. 2002).

73 This work is dedicated to the analysis of the peculiarities of the GdnHCl-induced
74 unfolding – refolding reactions of the recombinant bOBP and its monomeric mutants, bOBP-
75 Gly121+ and bOBP-Gly121+/W64C/H155C (GCC-bOBP). It continues a series of articles
76 dedicated to the analysis of the effect of the environment (including the presence of crowding
77 agents) on structural properties and conformational stability of bOBP. The mutant protein
78 bOBP-Gly121+ contains an extra glycine residue introduced after the bOBP residue 121.
79 This substitution was shown to promote monomerization of the bOBP (Stepanenko et al.
80 2015) likely via increasing the mobility of the loop connecting α-helix and 8th β-strand of the
81 β-barrel. Substitutions of the residues Trp64 and His156 to cysteines in bOBP-Gly121+
82 generate a mutant form GCC-bOBP, which is expected to have stable monomeric structure
83 due to the restoration of the disulfide bond typically seeing in other OBPs (Ramoni et al.
84 2008). We also investigated the role of the natural ligand in the stabilization of protein
85 structure and looked at how the ligand binding affected the folding-unfolding reaction of
86 these proteins.

87

MATHERIAL AND METHODS

Materials

GdnHCl (Nacalai Tesque, Japan), 1-octen-3-ol (OCT; Sigma-Aldrich, USA) and ANS (ammonium salt of 8-anilinonaphtalene-1-sulfonic acid; Fluka, Switzerland) were used without further purification. The protein concentration was 0.1 – 0.2 mg/ml. The OCT concentration was 10 mM. The experiments were performed in 20 mM Na-phosphate-buffered solution at pH 7.8.

Gene expression and protein purification

The plasmids pT7-7-bOBP which encodes bOBP and its mutant forms with a poly-histidine tag were used to transform *Escherichia coli* BL21(DE3) host (Invitrogen) (Stepanenko et al. 2014c). The protein expression was induced by incubating the cells with 0.3 mM of isopropyl-beta-D-1-thiogalactopyranoside (IPTG; Fluka, Switzerland) for 24 h at 37 °C. The recombinant protein was purified with Ni+-agarose packed in HisGraviTrap columns (GE Healthcare, Sweden). The protein purity was determined through SDS-PAGE in 15% polyacrylamide gel (Laemmli 1970).

Fluorescence spectroscopy

Fluorescence experiments were performed using a Cary Eclipse spectrofluorometer (Varian, Australia) with microcells FLR (10 x 10 mm; Varian, Australia). Fluorescence lifetime were measured using a “home built” spectrofluorometer with a nanosecond impulse (Stepanenko et al. 2014a; Stepanenko et al. 2012; Turoverov et al. 1998) as well as micro-cells (101.016-QS 5 x 5 mm; Hellma, Germany). Tryptophan fluorescence in the protein was excited at the long-wave

absorption spectrum edge (λ_{ex} = 297 nm), wherein the tyrosine residue contribution to the bulk protein fluorescence is negligible (Stepanenko et al. 2015). The fluorescence spectra position and form were characterized using the parameter $A = I_{320}/I_{365}$, wherein I_{320} and I_{365} are the fluorescence intensities at the emission wavelengths 320 and 365 nm, respectively (Turoverov & Kuznetsova 2003). The values for parameter *A* and the fluorescence spectrum were corrected for instrument sensitivity. The tryptophan fluorescence anisotropy was calculated using the equation: $r = (I_V^V - GI_H^V)/(I_V^V + 2GI_H^V)$, wherein I_V^V and I_H^V are the vertical and horizontal fluorescence intensity components upon excitement by vertically polarized light. *G* is the relationship between the fluorescence intensity vertical and horizontal components upon excitement by horizontally polarized light $(G = I_V^H / I_H^H)$, λ_{em} = 365 nm (Turoverov et al. 1998). The fluorescence intensity for the fluorescent dye ANS was recorded at λ_{em} = 480 nm (λ_{ex} = 365 nm).

GdnHCl-induced unfolding

Protein unfolding was initiated by manually mixing the protein solution (40 μL) with a buffer solution (510 μL) so that the GdnHCl concentration was varied from 0.0 to 4.0 – 5.0 M in the absence or presence of a natural ligand, 1-Octen-3-ol (OCT). The GdnHCl concentration was determined by the refraction coefficient using an Abbe refractometer (LOMO, Russia; (Pace 1986)). The dependences of different fluorescent characteristics of the studied proteins on GdnHCl were recorded following protein incubation in a solution with the appropriate denaturant concentration at 4ºC for different times (see in the text). The protein refolding was initiated by diluting the pre-denatured protein (in 3.0 M GdnHCl, 40 μL) with the buffer or denaturant solutions at various concentrations (510 μL). The spectrofluorimeter was equipped with a

thermostat that holds the temperature constant at 23°C.

Fitting of denaturation curves

The equilibrium dependences of the fluorescence intensity at 320 nm on the GdnHCl concentration were fit using a two-state model:

$$S = \frac{S_N + S_U K_{N-U}}{1 + K_{N-U}}, \quad (1)$$

$$K_{N-U} = \exp\left(\frac{-\Delta G^0_{N-U} + m_{N-U}[D]}{RT}\right), \quad (2)$$

$$K_{N-U} = F_U / F_N = (1 - F_N)/F_N, \quad (3)$$

taking into account

$$S_N = a_N + b_N[D], \quad (4)$$

$$S_U = a_U + b_U[D], \quad (5)$$

where S is the fluorescence intensity at the measured GdnHCl concentration; [D] is the guanidine concentration; m is the linear dependence of $\Delta G_{N\text{-}U}$ on the denaturant concentration; ΔG^0_{N-U} is the free energy of unfolding at 0 M denaturant; F_N and F_U are the fractions of native and unfolded molecules, respectively; and S_N and S_U are the signal of the native and unfolded states, respectively; a_N, b_N, a_U and b_U are constants needed to fit linear dependences of the S_N and S_U signals on the GdnHCl concentration. Fitting was performed using a nonlinear regression with Sigma Plot.

To evaluate conformational stability of the studied proteins we took into account that the formation of the native dimeric state of bOBP occurred at moderate GdnHCl concentration is

151 followed by full protein unfolding while conformational perturbations of bOBP at low denaturant
152 concentrations were not attributed to the unfolding of the protein globule (see "Results and
153 Discussion" section). As bOBP unfolding is fully reversible the transition from native to unfolded
154 state of the protein was used to calculate $\Delta G_{N\text{-}U}$ value. Conformational stability of the bOBP mutant
155 forms was evaluated similarly taking into account that both mutant proteins unfold through the
156 same scheme as bOBP does (see "Results and Discussion" section).

157

158 *Circular dichroism measurements*

159 The CD spectra were generated using a Jasco-810 spectropolarimeter (Jasco, Japan). Far-
160 UV CD spectra were recorded in a 1-mm path length cell from 260 nm to 190 nm with a 0.1 nm
161 step size. For the spectra, we generated 3 scans on average. The CD spectra for the appropriate
162 buffer solution were recorded and subtracted from the protein spectra.

163

164 *Gel filtration experiments*

165 We performed gel filtration experiments for recombinant bOBPwt and its mutant forms in a
166 buffered solution and with addition of GdnHCl using a Superdex-75 PC 3.2/30 column (GE
167 Healthcare, Sweden) and an AKTApurifier system (GE Healthcare, Sweden). The column was
168 equilibrated with the buffered solution or GdnHCl at the desired concentration, and 10 μl of the
169 protein solution prepared under the same conditions was loaded on the pre-equilibrated column.
170 The change in hydrodynamic dimensions for the studied proteins was evaluated as a change in the
171 protein elution volume. Multiple proteins with known molecular masses (aprotinin (6.5 kDa),
172 ribonuclease (13.7 kDa), carbonic anhydrase (29 kDa), ovalbumin (43 kDa) and conalbumin (75

kDa), which are chromatography standards from GE Healthcare) were used to generate the calibration curve.

RESULTS AND DISCUSSION

Structural features of the monomeric and dimeric bOBPs

Figure 1 compares structural features of the natural bOBP and its monomeric mutant GCC-bOBP. Structures shown in Figures 1A and 1B indicate that the domain swapping has been reverted in monomeric GCC-bOBP. Furthermore, Figure 1C represents the results of the multiple structural alignment of the one of the monomers of the natural dimeric bOBP (blue structure), monomeric mutant GCC-bOBP (red structure), and naturally monomeric pOBP (green structure) and clearly shows that the monomeric GCC-bOBP has the overall fold almost identical to that of the pOBP. Next, we analyzed how introduced mutations affected the structural flexibility of bOBP utilizing the power of the FlexPred tool that rapidly predicts absolute per-residue fluctuations from a three-dimensional structure of a query protein (Jamroz et al. 2012). Results of this analysis are shown in Figure 1D which clearly indicates that the chains of the bOBP dimer, chains of the naturally monomeric pOBP and the monomeric mutant GCC-bOBP are all characterized by very similar structural flexibility. Since the FlexPred tool provides real-value fluctuations of globular proteins based on their static structures by considering Cα atoms contact number and known B-factor values, the fact that these three proteins, bOBP (PDB ID: 1OBP), GCC-bOBP (PDB ID: 2HLV), and pOBP (PDB ID: 1A3Y), are predicted to have similar structural flexibility indicates that mutations introduced to generate the monomeric GCC-bOBP or present in the naturally

195 monomeric pOBP do not dramatically affect Cα atoms contact number and B-factors of the
196 resulting structures. Note that these observations are in a good agreement with the overall very
197 high structural similarity of these three proteins, the observation supported by the fact that the
198 multiple structural alignment of these three proteins over 136 residues was characterized by the
199 RMSD of 0.89 Å (see Figure 1C). We also compared these results of structure-based flexibility of
200 the bOBP with the propensity of this protein for intrinsic disorder evaluated by PONDR® VSL2B,
201 which is one of the more accurate stand-alone disorder predictors (Fan & Kurgan 2014; Peng et
202 al. 2005; Peng & Kurgan 2012). Results of this analysis are also shown in Figure 1D which
203 illustrates that there is generally a very good agreement between the structural flexibility calculated
204 from the protein crystal structure and the propensity of a protein for intrinsic disorder.

205

206 *Equilibrium unfolding of the recombinant bOBP in the presence of natural ligand*

207 Previously we have shown that the recombinant bOBP, unlike the natural bOBP extracted
208 from the tissues, represents a mixture of monomeric and dimeric forms suggesting that this protein
209 exists in a stable native-like state with a reduced dimerization capability (Stepanenko et al. 2014c).
210 It has been suggested that the recombinant form of bOBP is characterized by the disturbed package
211 of the α-helical region and some β-strands, which prevents the formation of a native domain-
212 swapped dimer (Stepanenko et al. 2014c). It is likely that the dimer formation via the domain
213 exchange mechanism is a rather complex process that requires specific organization of the
214 secondary and tertiary structure within the monomers. Curiously, recombinant bOBP can form the
215 compact dimeric state under the mild denaturing conditions, namely, in the presence of 1.5 M
216 guanidine hydrochloride (GdnHCl) (Stepanenko et al. 2014c). This process requires bOBP
217 restructuring and is accompanied by the formation of a stable, more compact, intermediate state

that is maximally populated at 0.5 M GdnHCl. Noticeably, at GdnHCl concentrations lower than 1.6 M we observed moderate changes in bOBP intrinsic fluorescence and far-UV CD spectra. These changes are not attributed to the bOBP unfolding process but are determined by some local structural changes in the protein globule. The dimeric bOBP in the presence of 1.5 M GdnHCl is characterized by a highly ordered secondary structure and a highly rigid microenvironment around the tryptophan residues. In the absence of GdnHCl, the recombinant bOBP is in a stable state with features similar to the native dimeric bOBP. Still, recombinant bOBP in the absence of GdnHCl is characterized by a less ordered secondary structure compared to the wild-type bOBP crystallographic data and a more rigid microenvironment of tryptophan residues, which is characterized by a decreased capacity of the recombinant bOBP for dimerization in aqueous solutions. This stable state of the recombinant bOBP state was designated as a "trapped" conformation with incorrect packing of α-helices and β-sheet within the protein globule, which may interfere with the formation of the bOBP native state. The reasons for accumulation of this "trapped" state may lie in a relatively complex domain-swapping dimerization mechanism which is also required for the monomers to be correctly folded. On the other hand, the intermediate state of bOBP structure which is accumulated at 0.5 M GdnHCl is characterized by the reorganized bOBP structure that has fewer elements of ordered secondary structure, compared with the recombinant bOBP structure both in an aqueous solution and in the solution containing 1.5 M GdnHCl. The increase of the GdnHCl concentration above 1.5 M induces cooperative unfolding of the recombinant bOBP, which is completed by ~3 M GdnHCl and is indicated by the simultaneous changes of all structural parameters of bOBP analyzed in this study (Stepanenko et al. 2014c). The half-transition point of this unfolding process at > 2 M GdnHCl indicates high conformational stability of the recombinant bOBP (Stepanenko et al. 2014c), which is comparable

241 with the stabilisites of the native (isolated from tissue) bOBP (Mazzini et al. 2002) and pOBP
242 (Staiano et al. 2007; Stepanenko et al. 2008) and is inherent to β-rich proteins (Stepanenko et al.
243 2012; Stepanenko et al. 2013; Stepanenko et al. 2014b). We have also established that the
244 unfolding of recombinant protein is a completely reversible process, whereas the preceding process
245 of the dimerization of recombinant bOBP is the irreversible event (Stepanenko et al. 2014c).

246 To understand how interaction of the recombinant bOBP with its natural ligand, 1-Octen-3-
247 ol (OCT) affects this protein, we investigated structural properties and conformational stability of
248 the recombinant bOBP in the presence and absence of OCT. The formation of the protein-ligand
249 complex does not affect the oligomeric status of the protein, since according to the gel filtration
250 analysis the protein in the bOBP/OCT complex continue to exist as a mixture of monomeric and
251 dimeric molecules. However, both monomeric and dimeric forms of the protein become more
252 compact as a result of the OCT binding (Table 1, Figure 2). The GdnHCl-induced unfolding of the
253 bOBP/OCT complex is a rather slow process, since the equilibrium unfolding curves are achieved
254 after incubation of the bOBP/OCT in the presence of different concentrations of the denaturing
255 agent for more than 24 hours. However, the established equilibrium was not affected by further
256 incubation for up to 5 days (Figure 3).

257 Figure 3 shows that the complexity of the bOBP/OCT unfolding is clearly illustrated by the
258 complex shapes of the equilibrium dependencies of various characteristics of this complex on
259 GdnHCl concentration. This suggests the accumulation of several intermediate states, which are
260 similar to partially folded species found during the equilibrium unfolding of the recombinant bOBP
261 in the absence of OCT. However, compared to the bOBP alone, in the case of the unfolding of
262 bOBP/OCT complex, the accumulation of these intermediate states takes place at higher
263 denaturant concentrations. In fact, a more compact intermediate state of the bOBP/OCT complex

264 is formed in the concentration range of 0.26 - 1.0 M GdnHCl, whereas the transition of the
265 bOBP/OCT complex to the dimeric state occurs only at 2.0 M GdnHCl (Figure 2). Increasing the
266 GdnHCl concentration over 2.0 M leads to the cooperative unfolding of the bOBP/OCT complex.
267 In comparison with the unfolding of the recombinant bOBP alone, the unfolding of the bOBP/OCT
268 complex occurs in a narrow concentration range, and higher denaturant concentrations are required
269 for complete unfolding of this complex. All these data indicate that formation of the bOBP/OCT
270 complex leads to the substantial stabilization of the protein, but does not affect its unfolding
271 mechanism.

272 To better understand the GdnHCl-induced unfolding of the bOBP/OCT complex, we
273 analyzed the dependence of the 8-anilinonaphthalene-1-sulfonic acid (ANS, also called 1-anilino-
274 8-naphthalenesulfonate), fluorescence on the denaturant concentration. This hydrophobic
275 fluorescent probe is frequently used for the analysis of the presence of solvent-exposed
276 hydrophobic patches in a protein (Stryer 1965) and for the detection of accumulation of partially
277 folded intermediates during equilibrium and kinetic protein unfolding-refolding processes due the
278 ability of ANS to bind to such solvent-exposed hydrophobic patches (which are commonly found
279 in partially folded proteins) and due to the fact that this interaction can be easily detected by the
280 significant increase in the ANS fluorescence intensity and a characteristic blue-shift of its
281 fluorescence maximum (Semisotnov et al. 1991). The shape of the unfolding curve monitored by
282 the GdnHCl-induced changes in the fluorescence intensity of ANS added to the bOBP/OCT was
283 remarkably different from the unfolding curve measured for the recombinant bOBP alone. We
284 observe a smooth continuous decrease in the ANS fluorescence intensity at moderate GdnHCl
285 concentrations, with the ANS fluorescence intensity reaching zero at the denaturant concentrations
286 leading to the formation of the compact dimeric form of bOBP (Figure 3).

These observations suggest that ANS interacts with bOBP at sites close to and/or overlapping with the ligand binding sites. Therefore, the formation of the bOBP/OCT complex prevents ANS binding. Earlier analysis of the dimeric bOBP structure revealed the presence of an additional ligand binding site at the interface between the monomeric subunits (Bianchet et al. 1996; Ikematsu et al. 2005; Pevsner et al. 1985). However, this inter-subunit binding site was shown to be noticeably weaker than the major ligand binding site located within the β-barrel (Bianchet et al. 1996; Ikematsu et al. 2005; Pevsner et al. 1985). Our data agree with the presence of an additional ligand binding site in a protein. At the formation of the dimeric bOBP/OCT complex with the native-like compactness at 2.0 M GdnHCl, this additional site is occupied by the ligand, also preventing its interaction with ANS.

Moderate ANS fluorescence is detected in solutions containing less than 2 M GdnHCl; i.e., under conditions where the bOBP/OCT complex exists as a mixture of monomeric and dimeric molecules, which are different from the native dimeric form of the bOBP. Under these conditions, ANS fluorescence intensity in the presence of the bOBP/OCT complex is noticeably lower than the ANS fluorescence recorded for the bOBP alone. These observations suggest that under these conditions the additional ligand binding site of the dimeric bOBP/OCT complex is occupied by ANS, whereas the inner cavity of the barrel is engaged in ligand binding. It is likely that the inability of the natural ligand to interact with the additional weak ligand binding site located between the monomeric subunits can be due to the structural difference of this site in the native dimeric bOBP and in a protein in the original native-like state or an intermediate compact state.

Analysis of the bOBP/OCT refolding from the completely unfolded state revealed that the dependencies of various structural characteristics of the bOBP/OCT on GdnHCl concentrations depend on the incubation time of this complex in the presence of the denaturant (see Figure 3). In

310 fact, during the refolding process, equilibrium values of the analyzed structural characteristics of
311 the bOBP/OCT complex are reached after the incubation of this complex in the presence of the
312 desired GdnHCl concentration for 72 hrs. No subsequent changes were detected when protein was
313 incubated for 30 days. This analysis revealed the presence of noticeable hysteresis between the
314 curves describing the equilibrium unfolding and refolding of the bOBP/OCT complex in a wide
315 range of the GdnHCl concentrations. In fact, the equilibrium unfolding and refolding curves
316 coincide only in the vicinity of 2.0 M GdnHCl, where, according to the gel-filtration analysis, the
317 native dimeric state of the bOBP/OCT complex is formed, whereas within the region
318 corresponding to the transition from the native dimeric form to the completely unfolded state of
319 the bOBP/OCT complex, equilibrium curves describing unfolding and refolding of this complex
320 do not coincide.

321 The equilibrium refolding curve describing transition from the unfolded to the compact
322 dimeric state of the bOBP/OCT complex is shifted toward the lower GdnHCl concentrations in
323 comparison with the equilibrium unfolding curve (Figure 3). However, in comparison with the
324 unfolding of the bOBP alone, this equilibrium refolding curve of the bOBP/OCT complex is still
325 shifted toward higher GdnHCl concentrations. These data suggest that at the same denaturant
326 concentrations, the fractions of native bOBP formed during the refolding from the completely
327 unfolded state are significantly lower than the fraction of native protein remaining within the
328 region of the bOBP/OCT unfolding. However, once formed, the native protein gains the ability to
329 bind ligand. This hypothesis is supported by the results of the gel-filtration analysis (Figure 2). For
330 example, the elution profiles registered during the unfolding and refolding of the bOBP/OCT
331 complex at 2.5 M GdnHCl show that under these conditions, more native protein is present during
332 the bOBP/OCT unfolding, whereas unfolded species prevail during the refolding of this complex.

333 Therefore, the effective rates of the formation of various bOBP conformers are significantly
334 different during the unfolding and refolding processes and noticeably depend on the denaturant
335 concentration.

336 It is likely that the same reasons define the irreversibility of the unfolding of the bOBP/OCT
337 complex at low GdnHCl concentrations. Under these conditions, the rate of the formation of the
338 monomeric bOBP/OCT complex is significantly higher than the rate of the dimeric bOBP/OCT
339 formation. As a result, refolding of the bOBP/OCT complex at the low GdnHCl concentrations
340 results in the preferential formation of monomeric bOBP/OCT species, whereas under the identical
341 conditions, the unfolding reaction mixture contains roughly equimolar quantities of the
342 bOBP/OCT monomers and dimers (Figures 2 and 3).

343

344 *Equilibrium unfolding of the monomeric bOBP-Gly121+*

345 Already at relatively low GdnHCl concentrations, the monomeric bOBP-Gly121+ is
346 converted to the compact partially folded state with structural characteristics resembling those of
347 the partially folded species accumulated during the equilibrium unfolding of the recombinant
348 bOBP (see Figures 4, 5 and Table 1). This compact intermediate is able to bind ANS and exists in
349 a wide range of the GdnHCl concentrations (up to about 1.3 M GdnHCl). Subsequent increase in
350 the denaturant concentration promotes transition to a more loose form, which, at the further
351 increase of the GdnHCl concentration, is converted to the completely unfolded state. This
352 GdnHCl-induced unfolding of the bOBP-Gly121+ is a completely reversible process as evidenced
353 by the coincidence of the equilibrium characteristics of the protein measured at the processes of
354 the bOBP-Gly121+ unfolding and refolding.

355 The formation of the bOBP-Gly121+/OCT complex results in a noticeable stabilization of
356 this protein. This is evidenced by the increase in the cooperativity of the unfolding transition,
357 which is also shifted toward higher GdnHCl concentrations. However, the formation of a complex
358 between the bOBP-Gly121+ and OCT does not affect the unfolding mechanism of this protein.

359

360 *GdnHCl-induced unfolding of the monomeric GCC-bOBP*

361 Analysis of the peculiarities of the equilibrium unfolding and refolding processes monitored
362 by the GdnHCl-induced changes in various structural characteristics of the monomeric GCC-
363 bOBP suggests that the unfolding of this protein is a completely reversible process accompanied
364 by the formation of partially folded intermediates similar to those observed during the equilibrium
365 unfolding of the recombinant bOBP and its monomeric bOBP-Gly121+ form (see Figures 6, 7 and
366 Table 1). However, although qualitatively unfolded processes of these three proteins are similar,
367 there are some noticeable differences. For example, in comparison with the recombinant bOBP
368 and bOBP-Gly121+ unfolding, a compact intermediate with high ANS affinity is formed at higher
369 denaturant concentrations during the GCC-bOBP unfolding (at 1.0 M GdnHCl). This illustrates
370 higher conformational stability of the disulfide-stabilized GCC-bOBP compared to the
371 recombinant bOBP and its monomeric form bOBP-Gly121+.

372 GCC-bOBP is further stabilized due to the GCC-bOBP/OCT complex formation. Refolding
373 curves detected by changes in different structural characteristics of this complex and registered
374 after the incubation of the corresponding solutions for one hour coincide with the transition curves
375 describing the equilibrium unfolding of GCC-bOBP, and subsequent incubation of these same
376 solutions for 72 hrs leads to the detectable shift of the transition curves. As a result, equilibrium
377 unfolding and refolding transitions of the GCC-bOBP/OCT complex coincide suggesting that the

unfolding of this protein is a completely reversible process. However, GCC-bOBP becomes able to bind ligand only after the formation of correct native structure stabilized by the disulfide bond. Earlier similar effects were described for other ligand-binding protein, such as the D-glucose/D-galactose-binding protein (GGBP) from *E. coli* (Stepanenko et al. 2011a; Stepanenko et al. 2009; Stepanenko et al. 2011b). In fact, our analysis of the peculiarities of the GGBP unfolding revealed that ligand binding might constitute a rate-limiting stage of the protein unfolding-refolding process. This phenomenon can be understood considering the fact that the formation of the protein-ligand complex depends on the appearance of the matching configurations between the ligand and the active site of a fully formed native protein (Stepanenko et al. 2011a; Stepanenko et al. 2009; Stepanenko et al. 2011b).

Our current analysis revealed that the unfolding of the monomeric complexes bOBP-Gly121+/OCT and GCC-bOBP/OCT is not accompanied by the ANS fluorescence enhancement in the whole range of GdnHCl concentrations (see Figures 5 and 7). These observations support the hypothesis on the existence of the additional ligand-binding site in the dimeric bOBP.

Table 2 shows that the equilibrium unfolding transition recorded for the recombinant bOBP coincides with that of its monomeric bOBP-Gly121+ form. On the other hand, unfolding transition of the monomeric GCC-bOBP stabilized by the engineered disulfide bond is noticeably shifted to higher denaturant concentrations. Curiously, the unfolding of complexes of all proteins analyzed in this study with natural ligand OCT happens at the same denaturant concentrations.

It is important to note here that the quantitative characterization of the affinity of the bOBP and its mutants to the natural OCT ligand is beyond the scope of this study. In fact, the binding constant of the protein was determined in previous studies (Bianchet et al. 1996; Ikematsu et al. 2005; Pevsner et al. 1985). According to published data, binding constant of a natural OCT ligand

401 to the triple mutant GCC-bOBP is in the micromolar range, which is similar to the affinity of the
402 wild type protein (Ramoni et al. 2008). Amino acid substitutions introduced in mutant proteins,
403 namely the Gly 121+ insertion and the W64C and H155C replacements, do not affect the ligand-
404 binding site of the protein. Data reported in the first paper of this series (Stepanenko et al. 2015)
405 revealed that these substitutions do not have significant influence on the protein tertiary and
406 secondary structure. All these data indicate that the mutant forms of the bOBP protein might retain
407 affinity inherent to the wild-type protein.

408 Our data suggest that protein dimerization via the domain-swapping mechanism does not
409 contribute much to the increase in the conformational stability of a protein (at least in the case of
410 the analyzed in this study bOBP), despite the fact that the increased conformational stability was
411 proposed as one of the factors determining the use of this mechanism for dimer and higher
412 oligomer formation (Bennett et al. 1995; Liu & Eisenberg 2002). In contrast, introduction of a
413 disulfide bond to the structure of a monomeric protein shows significant stabilizing effects. Our
414 data also show that the formation of a protein-ligand complex leads to the significant stabilization
415 of different variants of bOBP and eliminates the original difference in conformational stability
416 caused by their structural differences.

417

418 **DISCLOSURE**

419 None declared.

REFERENCES

Bennett MJ, Schlunegger MP, and Eisenberg D. 1995. 3D domain swapping: a mechanism for oligomer assembly. *Protein Sci* 4:2455-2468.

Bianchet MA, Bains G, Pelosi P, Pevsner J, Snyder SH, Monaco HL, and Amzel LM. 1996. The three-dimensional structure of bovine odorant binding protein and its mechanism of odor recognition. *Nat Struct Biol* 3:934-939.

Bignetti E, Cavaggioni A, Pelosi P, Persaud KC, Sorbi RT, and Tirindelli R. 1985. Purification and characterisation of an odorant-binding protein from cow nasal tissue. *Eur J Biochem* 149:227-231.

Bignetti E, Damiani G, De Negri P, Romani R, Avanzini F, Ferrari G, and Rossi GL. 1987. Specificity of an immunoaffinity column for odorant-binding protein from bovine nasal mucosa. *Chem Senses* 12:601-608.

Boudjelal M, Sivaprasadarao A, and Findlay JB. 1996. Membrane receptor for odour-binding proteins. *Biochem J* 317 (Pt 1):23-27.

Briand L, Eloit C, Nespoulous C, Bezirard V, Huet JC, Henry C, Blon F, Trotier D, and Pernollet JC. 2002. Evidence of an odorant-binding protein in the human olfactory mucus: location, structural characterization, and odorant-binding properties. *Biochemistry* 41:7241-7252.

D'Auria S, Staiano M, Varriale A, Scognamiglio V, Rossi M, Parracino A, Campopiano S, Cennamo N, and Zeni L. 2006. The odorant-binding protein from Canis familiaris: purification, characterization and new perspectives in biohazard assessment. *Protein Pept Lett* 13:349-352.

Dal Monte M, Andreini I, Revoltella R, and Pelosi P. 1991. Purification and characterization of two odorant-binding proteins from nasal tissue of rabbit and pig. *Comp Biochem Physiol B* 99:445-451.

Dutta S, Burkhardt K, Young J, Swaminathan GJ, Matsuura T, Henrick K, Nakamura H, and Berman HM. 2009. Data deposition and annotation at the worldwide protein data bank. *Mol Biotechnol* 42:1-13.

Fan X, and Kurgan L. 2014. Accurate prediction of disorder in protein chains with a comprehensive and empirically designed consensus. *J Biomol Struct Dyn* 32:448-464.

Flower DR, North AC, and Sansom CE. 2000. The lipocalin protein family: structural and sequence overview. *Biochim Biophys Acta* 1482:9-24.

Grzyb J, Latowski D, and Strzalka K. 2006. Lipocalins - a family portrait. *J Plant Physiol* 163:895-915.

Hsin J, Arkhipov A, Yin Y, Stone JE, and Schulten K. 2008. Using VMD: an introductory tutorial. *Curr Protoc Bioinformatics* Chapter 5:Unit 5 7.

Ikematsu M, Takaoka D, and Yasuda M. 2005. Odorant binding initially occurring at the central pocket in bovine odorant-binding protein. *Biochem Biophys Res Commun* 333:1227-1233.

Jamroz M, Kolinski A, and Kihara D. 2012. Structural features that predict real-value fluctuations of globular proteins. *Proteins* 80:1425-1435.

Laemmli UK. 1970. Cleavage of structural proteins during the assembly of the head of bacteriophage T4. *Nature* 227:680-685.

Liu Y, and Eisenberg D. 2002. 3D domain swapping: as domains continue to swap. *Protein Sci* 11:1285-1299.

Mazzini A, Maia A, Parisi M, Sorbi RT, Ramoni R, Grolli S, and Favilla R. 2002. Reversible unfolding of bovine odorant binding protein induced by guanidinium hydrochloride at neutral pH. *Biochim Biophys Acta* 1599:90-101.

Merritt EA, and Bacon DJ. 1977. Raster3D: Photorealistic molecular graphics. . *Methods enzymol* 277:505-524.

Nolting B. 1999. Protein folding kinetics. In Biophysical Methods, p 111, Springer-Verlag, Berlin-Heidelberg.

Pace CN. 1986. Determination and analysis of urea and guanidine hydrochloride denaturation curves. *Methods Enzymol* 131:266-280.

Pelosi P, Baldaccini NE, and Pisanelli AM. 1982. Identification of a specific olfactory receptor for 2-isobutyl-3-methoxypyrazine. *Biochem J* 201:245-248.

Peng K, Vucetic S, Radivojac P, Brown CJ, Dunker AK, and Obradovic Z. 2005. Optimizing long intrinsic disorder predictors with protein evolutionary information. *J Bioinform Comput Biol* 3:35-60.

Peng ZL, and Kurgan L. 2012. Comprehensive comparative assessment of in-silico predictors of disordered regions. *Curr Protein Pept Sci* 13:6-18.

Pevsner J, and Snyder SH. 1990. Odorant-binding protein: odorant transport function in the vertebrate nasal epithelium. *Chem Senses* 15:217-222.

Pevsner J, Trifiletti RR, Strittmatter SM, and Snyder SH. 1985. Isolation and characterization of an olfactory receptor protein for odorant pyrazines. *Proc Natl Acad Sci U S A* 82:3050-3054.

Ramoni R, Spinelli S, Grolli S, Conti V, Merli E, Cambillau C, and Tegoni M. 2008. Deswapping bovine odorant binding protein. *Biochim Biophys Acta* 1784:651-657.

Ramoni R, Vincent F, Ashcroft AE, Accornero P, Grolli S, Valencia C, Tegoni M, and Cambillau C. 2002. Control of domain swapping in bovine odorant-binding protein. *Biochem J* 365:739-748.

Semisotnov GV, Rodionova NA, Razgulyaev OI, Uversky VN, Gripas AF, and Gilmanshin RI. 1991. Study of the "molten globule" intermediate state in protein folding by a hydrophobic fluorescent probe. *Biopolymers* 31:119-128.

Shatsky M, Nussinov R, and Wolfson HJ. 2004. A method for simultaneous alignment of multiple protein structures. *Proteins* 56:143-156.

Spinelli S, Ramoni R, Grolli S, Bonicel J, Cambillau C, and Tegoni M. 1998. The structure of the monomeric porcine odorant binding protein sheds light on the domain swapping mechanism. *Biochemistry* 37:7913-7918.

Staiano M, D'Auria S, Varriale A, Rossi M, Marabotti A, Fini C, Stepanenko OV, Kuznetsova IM, and Turoverov KK. 2007. Stability and dynamics of the porcine odorant-binding protein. *Biochemistry* 46:11120-11127.

Stepanenko OV, Bublikov GS, Stepanenko OV, Shcherbakova DM, Verkhusha VV, Turoverov KK, and Kuznetsova IM. 2014a. A knot in the protein structure - probing the near-infrared fluorescent protein iRFP designed from a bacterial phytochrome. *Febs J* 281:2284-2298.

Stepanenko OV, Fonin AV, Stepanenko OV, Morozova KS, Verkhusha VV, Kuznetsova IM, Turoverov KK, Staiano M, and D'Auria S. 2011a. New insight in protein-ligand interactions. 2. Stability and properties of two mutant forms of the D-galactose/D-glucose-binding protein from E. coli. *J Phys Chem B* 115:9022-9032.

511 Stepanenko OV, Fonin AV, Stepanenko OV, Staiano M, D'Auria S, Kuznetsova IM, and
512 Turoverov KK. 2015. Tryptophan residue of the D-galactose/D-glucose-binding protein
513 from E. Coli localized in its active center does not contribute to the change in intrinsic
514 fluorescence upon glucose binding. *J Fluoresc* 25:87-94.
515 Stepanenko OV, Marabotti A, Kuznetsova IM, Turoverov KK, Fini C, Varriale A, Staiano M,
516 Rossi M, and D'Auria S. 2008. Hydrophobic interactions and ionic networks play an
517 important role in thermal stability and denaturation mechanism of the porcine odorant-
518 binding protein. *Proteins* 71:35-44.
519 Stepanenko OV, Povarova OI, Stepanenko OV, Fonin AV, Kuznetsova IM, Turoverov KK,
520 Staiano M, and D'Auria S. 2009. Structure and stability of D-galactose/D-glucose-
521 binding protein. The role of D-glucose binding and Ca ion depletion. *Spectrosc Biomed*
522 *Appl* 24 355-359.
523 Stepanenko OV, Stepanenko OV, Kuznetsova IM, Shcherbakova DM, Verkhusha VV, and
524 Turoverov KK. 2012. Distinct effects of guanidine thiocyanate on the structure of
525 superfolder GFP. *PLoS One* 7:e48809.
526 Stepanenko OV, Stepanenko OV, Kuznetsova IM, Verkhusha VV, and Turoverov KK. 2013.
527 Beta-barrel scaffold of fluorescent proteins: folding, stability and role in chromophore
528 formation. *Int Rev Cell Mol Biol* 302:221-278.
529 Stepanenko OV, Stepanenko OV, Kuznetsova IM, Verkhusha VV, and Turoverov KK. 2014b.
530 Sensitivity of superfolder GFP to ionic agents. *PLoS One* 9:e110750.
531 Stepanenko OV, Stepanenko OV, Povarova OI, Fonin AV, Kuznetsova IM, Turoverov KK,
532 Staiano M, Varriale A, and D'Auria S. 2011b. New insight into protein-ligand
533 interactions. The case of the D-galactose/D-glucose-binding protein from Escherichia
534 coli. *J Phys Chem B* 115:2765-2773.
535 Stepanenko OV, Stepanenko OV, Staiano M, Kuznetsova IM, Turoverov KK, and D'Auria S.
536 2014c. The quaternary structure of the recombinant bovine odorant-binding protein is
537 modulated by chemical denaturants. *PLoS One* 9:e85169.
538 Stepanenko OV, Roginskii DO, Stepanenko OV, Kuznetsova IM, Uversky VN, and Turoverov
539 KK. 2015. Structure and stability of recombinant bovine odorant-binding protein: I.
540 Design and analysis of monomeric mutants. *PeerJ*. Submitted.
541 Stryer L. 1965. The interaction of a naphthalene dye with apomyoglobin and apohemoglobin. A
542 fluorescent probe of non-polar binding sites. *J Mol Biol* 13:482-495.
543 Tegoni M, Ramoni R, Bignetti E, Spinelli S, and Cambillau C. 1996. Domain swapping creates a
544 third putative combining site in bovine odorant binding protein dimer. *Nat Struct Biol*
545 3:863-867.
546 Turoverov KK, Biktashev AG, Dorofeiuk AV, and Kuznetsova IM. 1998. [A complex of
547 apparatus and programs for the measurement of spectral, polarization and kinetic
548 characteristics of fluorescence in solution]. *Tsitologiia* 40:806-817.
549 Turoverov KK, and Kuznetsova IM. 2003. Intrinsic fluorescence of actin. *J Fluorescence* 13:41-
550 57.
551 Vincent F, Spinelli S, Ramoni R, Grolli S, Pelosi P, Cambillau C, and Tegoni M. 2000.
552 Complexes of porcine odorant binding protein with odorant molecules belonging to
553 different chemical classes. *J Mol Biol* 300:127-139.
554 Xu P, Atkinson R, Jones DN, and Smith DP. 2005. Drosophila OBP LUSH is required for
555 activity of pheromone-sensitive neurons. *Neuron* 45:193-200.

FIGURE LEGENDS

Figure 1. Analysis of the 3D structure of bOBP. Crystal 3D structures of natural bOBP (***A***) and monomeric mutant form GCC-bOBP (***B***). The individual subunits in the bOBP are in gray and orange. In the GCC-bOBP short α-helical segment that followed by the 9th β-strand and the disordered C-terminal region of the protein are drown in orange. The tryptophan residues are indicated in red and blue in the different subunits of bOBP and in blue in GCC-bOBP. The Gly 121+ residue which donates the increased mobility of the loop connecting α-helix and 8th β-strand of the β-barrel and promotes the formation of a monomeric fold of the mutant protein bOBP-Gly121+ is in green. Two cysteine residues Cys 64 and Cys 156 in GCC-bOBP, which are believed to stabilize monomeric structure due to the disulfide bond formation are shown in yellow. The drawing of bOBP and GCC-bOBP was generated based on the 1OBP (Tegoni et al. 1996) and 2HLV files (Ramoni et al. 2008) from PDB (Dutta et al. 2009) using the graphic software VMD (Hsin et al. 2008) and Raster3D (Merritt & Bacon 1977). Plot ***C*** represents the results of the multiple structural alignment of bOBP (PDB ID: 1OBP, blue structure), GCC-bOBP (PDB ID: 2HLV, red structure), and naturally monomeric pOBP (PDB ID: 1A3Y, green structure) using the MultiProt algorithm (http://bioinfo3d.cs.tau.ac.il/MultiProt/) (Shatsky et al. 2004). The drawing was generated using the graphic software VMD (Hsin et al. 2008). Plot ***D*** compares flexibility profiles obtained from crystal structures of bOBP (PDB ID: 1OBP, black and red lines for the chains A and B), naturally monomeric pOBP (PDB ID: 1A3Y, green and yellow lines for the chains A and B) and monomeric mutant GCC-bOBP (PDB ID: 2HLV, blue line) with the intrinsic disorder propensity of the bOBP (UniProt ID: P07435, pink dashed line). Flexibility profiles were obtained using the FlexPred software available at http://kiharalab.org/flexPred/ (Jamroz et al. 2012), whereas intrinsic disorder propensity of the bOBP (UniProt ID: P07435) was evaluated using the PONDR® VSL2 algorithm (Peng et al. 2005).

Figure 2. The changes of hydrodynamic dimensions of recombinant bOBP (*A* and *B*) and its complex with ligand bOBP/OCT (*C* and *D*) in different structural states. The elution profiles for bOBP and bOBP/OCT were recorded during the protein denaturation (***A*** and ***C***) and renaturation from unfolded states (***B*** and ***D***) induced by GdnHCl. The elution profiles for bOBP were measured after pre-incubation of the protein and the solution of GdnHCl in desired concentration for 24h (***A*** and ***B***), while in the case of bOBP/OCT the incubation time was extended to 72 – 84 h for denaturation (***C***) and 6 days for renaturation (***D***). The figures on the curves are the GdnHCl concentrations.

Figure 3. bOBP and bOBP/OCT conformational changes induced by GdnHCl. ***A***: changes in fluorescence intensity at 320 nm, λ_{ex}=297 nm; ***B***: changes in parameter *A*, λ_{ex}=297 nm; ***C***: changes in fluorescence anisotropy at the emission wavelength 365 nm, λ_{ex}=297 nm; ***D***: changes in the ellipticity at 222 nm; ***E***: changes in the ANS fluorescence intensity at λ_{ex}=365 nm, λ_{em}=480 nm. The statistical errors for fluorescence measurements were assessed and were shown to fall within the range of 0.2 - 1 %.
The measurements were preceded by incubating the protein in a solution with the appropriate GdnHCl concentration at 4ºC for 24 (red circles) in the case of bOBP. The open symbols indicate unfolding, whereas the closed symbols represent refolding. While studying the folding of bOBP/OCT (squares), the solution of complex of the protein with its ligand were incubated in a solution with the appropriate GdnHCl concentration at 4ºC for less than 24 h (open brown squares),

up to 120 h (open pink squares) at the protein denaturation, and 1 h (closed brown squares) and 72 h – 30 days (closed pink squares) at the protein renaturation.

Figure 4. The changes of hydrodynamic dimensions of recombinant bOBP-Gly121+ (*A* and *B*) and its complex with ligand bOBP-Gly121+/OCT (*C* and *D*) in different structural states. The elution profiles for bOBP-Gly121+ and bOBP-Gly121+/OCT were recorded during the protein denaturation (***A*** and ***C***) and renaturation from unfolded states (***B*** and ***D***) induced by GdnHCl. The elution profiles for bOBP-Gly121+ were measured after pre-incubation of the protein and the solution of GdnHCl in desired concentration for 24h (***A*** and ***B***), while in the case of bOBP-Gly121+/OCT the incubation time was extended to 72 – 84 h for denaturation (***C***) and 6 days for renaturation (***D***). The figures on the curves are the GdnHCl concentrations.

Figure 5. bOBP-Gly121+ and bOBP-Gly121+/OCT conformational changes induced by GdnHCl. ***A***: changes in fluorescence intensity at 320 nm, λ_{ex}=297 nm; ***B***: changes in parameter *A*, λ_{ex}=297 nm; ***C***: changes in fluorescence anisotropy at the emission wavelength 365 nm, λ_{ex}=297 nm; ***D***: changes in the ellipticity at 222 nm; ***E***: changes in the ANS fluorescence intensity at λ_{ex}=365 nm, λ_{em}=480 nm. The statistical errors for fluorescence measurements were assessed and were shown to fall within the range of 0.2 - 1 %.
The measurements were preceded by incubating the protein in a solution with the appropriate GdnHCl concentration at 4ºC for 24 (dark green circles) in the case of bOBP-Gly121+. The open symbols indicate unfolding, whereas the closed symbols represent refolding. While studying the folding of bOBP-Gly121+/OCT (squares), the solution of complex of the protein with its ligand were incubated in a solution with the appropriate GdnHCl concentration at 4ºC for less than 24 h (open dark yellow squares), up to 72 h (open light green squares) at the protein denaturation, and 1 h (closed dark yellow squares) and 72 h (closed light green squares) at the protein renaturation.

Figure 6. The changes of hydrodynamic dimensions of recombinant GCC-bOBP (*A* and *B*) and its complex with ligand GCC-bOBP/OCT (*C* and *D*) in different structural states. The elution profiles for GCC-bOBP and GCC-bOBP/OCT were recorded during the protein denaturation (***A*** and ***C***) and renaturation from unfolded states (***B*** and ***D***) induced by GdnHCl. The elution profiles for GCC-bOBP were measured after pre-incubation of the protein and the solution of GdnHCl in desired concentration for 24h (***A*** and ***B***), while in the case of GCC-bOBP/OCT the incubation time was extended to 72 – 84 h for denaturation (***C***) and 6 days for renaturation (***D***). The figures on the curves are the GdnHCl concentrations.

Figure 7. GCC-bOBP and GCC-bOBP/OCT conformational changes induced by GdnHCl. ***A***: changes in fluorescence intensity at 320 nm, λ_{ex}=297 nm; ***B***: changes in parameter *A*, λ_{ex}=297 nm; ***C***: changes in fluorescence anisotropy at the emission wavelength 365 nm, λ_{ex}=297 nm; ***D***: changes in the ellipticity at 222 nm; ***E***: changes in the ANS fluorescence intensity at λ_{ex}=365 nm, λ_{em}=480 nm. The statistical errors for fluorescence measurements were assessed and were shown to fall within the range of 0.2 - 1 %.
The measurements were preceded by incubating the protein in a solution with the appropriate GdnHCl concentration at 4ºC for 24 (blue circles) in the case of GCC-bOBP. The open symbols indicate unfolding, whereas the closed symbols represent refolding. While studying the folding of GCC-bOBP/OCT (squares), the solution of complex of the protein with its ligand were incubated in a solution with the appropriate GdnHCl concentration at 4ºC for less than 24 h (open dark blue

squares), up to 72 h (open light blue squares) at the protein denaturation, and 1 h (closed dark blue squares) and 72 h (closed light blue squares) at the protein renaturation.

Table 1(on next page)

Table 1

Hydrodynamic dimensions of recombinant bOBPwt and its mutant forms in the absence and in the presence of natural ligand OCT in different structural states.

Table 1. Hydrodynamic dimensions of recombinant bOBPwt and its mutant forms in the absence and in the presence of natural ligand OCT in different structural states.

	GdnHCl, M	First peak, kDa	Second peak, kDa
bOBPwt	0.0 0.5 1.5	43.9 34.0 43.6	23.8 19.3
bOBPwt/OCT	0.0 0.55 1.7	39.6 27.2 39.6	21.5 17.0
bOBP/Gly121+	0.0 0.25 1.5 – 1.9	23.6 17.8 24.8 – 28.5	
bOBP/Gly121+/OCT	0.0 0.24 – 0.5 1.7 – 2.0	21.5 15.5 – 16.2 24.7 – 28.5	
GCC-bOBP	0.0 0.25 1.1 – 1.82	23.6 17.8 22.5 – 25.9	
GCC-bOBP/OCT	0.0 0.27 1.5 – 2.0	22.5 16.9 22.5 – 27.2	

Table 2(on next page)

Table 2

Thermodynamic parameters of GdnHCl-induced denaturation of bOBP, its mutant variants and their complexes with octen-3-ol (OCT)

Table 2. Thermodynamic parameters of GdnHCl-induced denaturation of bOBP, its mutant variants and their complexes with octen-3-ol (OCT)

protein	m (kJ mol^{-1} M^{-1})	C_m (M)[a]	$\Delta G^0_{N\text{-}U}$ [b] (kJ mol^{-1})
bOBP	3.7 ± 0.2	2.1 ± 0.1	7.7 ± 0.6
bOBP/OCT	4.1 ± 0.2	2.7 ± 0.1	11.0 ± 0.5
bOBP/Gly121+	2.8 ± 0.2	2.0 ± 0.1	5.5 ± 0.4
bOBP/Gly121+/OCT	5.3 ± 0.2	2.6 ± 0.1	14.0 ± 0.5
GCC-bOBP	2.5 ± 0.3	2.3 ± 0.1	5.8 ± 0.7
GCC-bOBP/OCT	4.5 ± 0.3	2.7 ± 0.1	12.0 ± 0.9

[a] C_m is the denaturant concentration at midpoint of conformational transition

[b] The fluorescence signals of the folded and unfolded states were approximated by linear dependences as function of denaturant concentration (Nolting, 1999).

1

Analysis of the 3D structure of bOBP.

Crystal 3D structures of natural bOBP (***A***) and monomeric mutant form GCC-bOBP (***B***). The individual subunits in the bOBP are in gray and orange. In the GCC-bOBP short α-helical segment that followed by the 9th β-strand and the disordered C-terminal region of the protein are drown in orange. The tryptophan residues are indicated in red and blue in the different subunits of bOBP and in blue in GCC-bOBP. The Gly 121+ residue which donates the increased mobility of the loop connecting α-helix and 8th β-strand of the β-barrel and promotes the formation of a monomeric fold of the mutant protein bOBP-Gly121+ is in green. Two cysteines residues Cys 64 and Cys 156 in GCC-bOBP, which are believed to stabilize monomeric structure due to the disulfide bond formation are in yellow. The drawing of bOBP and GCC-bOBP was generated based on the 1OBP (Tegoni et al. 1996) and 2HLV files (Ramoni et al. 2008) from PDB (Dutta et al. 2009) using the graphic software VMD (Hsin et al. 2008) and Raster3D (Merritt & Bacon 1977). Plot ***C*** represents the results of the multiple structural alignment of bOBP (PDB ID: 1OBP, blue structure), GCC-bOBP (PDB ID: 2HLV, red structure), and naturally monomeric pOBP (PDB ID: 1A3Y, green structure) using the MultiProt algorithm (http://bioinfo3d.cs.tau.ac.il/MultiProt/) (Shatsky et al. 2004). The drawing was generated using the graphic software VMD (Hsin et al. 2008). Plot ***D*** compares flexibility profiles obtained from crystal structures of bOBP (PDB ID: 1OBP, black and red lines for the chains A and B), naturally monomeric pOBP (PDB ID: 1A3Y, green and yellow lines for the chains A and B) and monomeric mutant GCC-bOBP (PDB ID: 2HLV, blue line) with the intrinsic disorder propensity of the bOBP (UniProt ID: P07435, pink dashed line). Flexibility profiles were obtained using the FlexPred software available at http://kiharalab.org/flexPred/ (Jamroz et al. 2012), whereas intrinsic disorder propensity was evaluated using the PONDR® VSL2 algorithm (Peng et al. 2005).

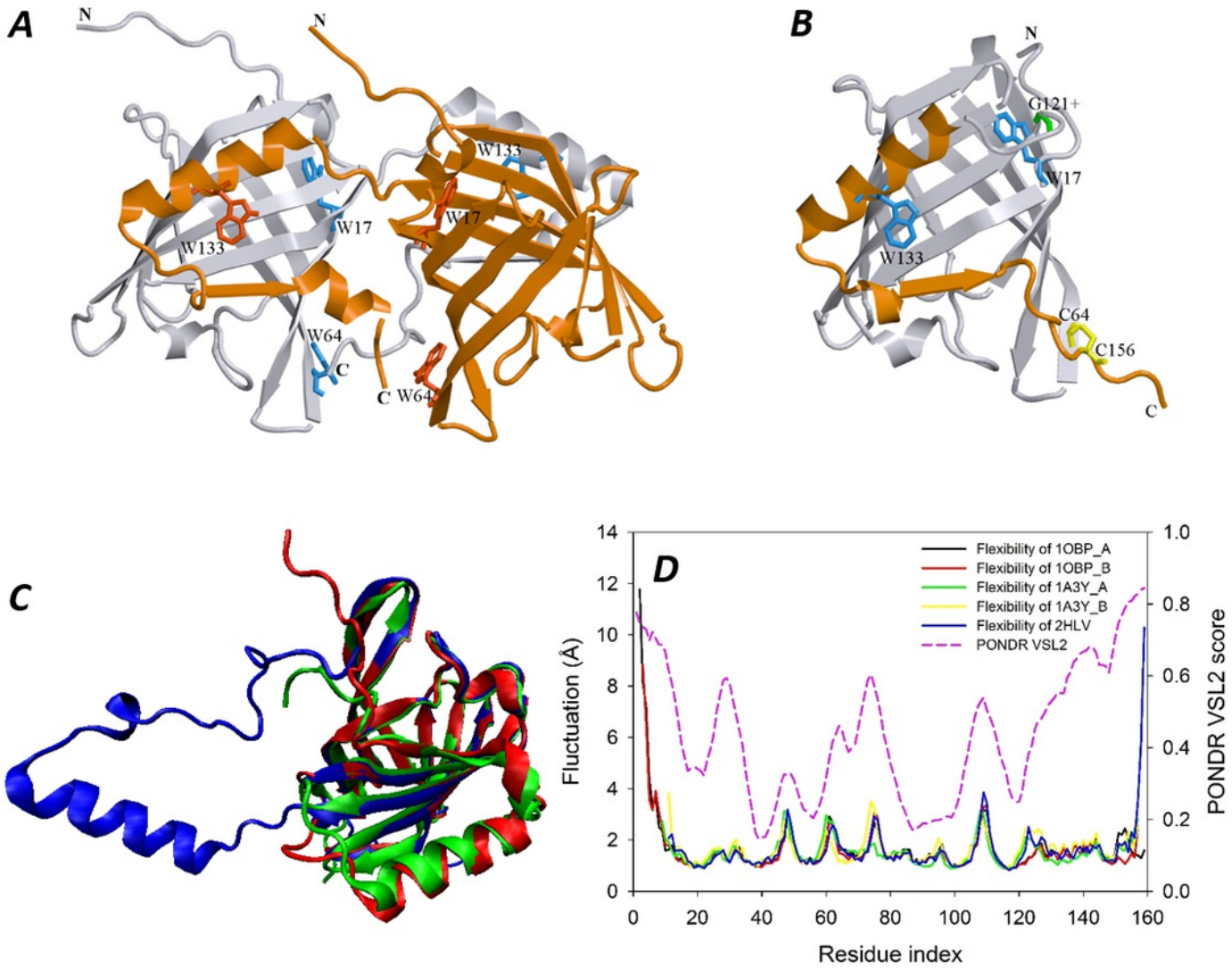
A
N
N
W133
W17
W17
W133
W64
C
C W64
B
N
G121+
W17
W133
C64
C156
C
C
D
Flexibility of 1OBP_A
Flexibility of 1OBP_B
Flexibility of 1A3Y_A
Flexibility of 1A3Y_B
Flexibility of 2HLV
PONDR VSL2
Fluctuation (Å)
PONDR VSL2 score
Residue index
0
2
4
6
8
10
12
14
0.0
0.2
0.4
0.6
0.8
1.0
0
20
40
60
80
100
120
140
160

2

The changes of hydrodynamic dimensions of recombinant bOBP (*A* and *B*) and its complex with ligand bOBP/OCT (*C* and *D*) in different structural states.

The elution profiles for bOBP and bOBP/OCT were recorded during the protein denaturation (***A*** and ***C***) and renaturation from unfolded states (***B*** and ***D***) induced by GdnHCl. The elution profiles for bOBP were measured after pre-incubation of the protein and the solution of GdnHCl in desired concentration for 24h (***A*** and ***B***), while in the case of bOBP/OCT the incubation time was extended to 72 – 84 h for denaturation (***C***) and 6 days for renaturation (***D***). The figures on the curves are the GdnHCl concentrations.

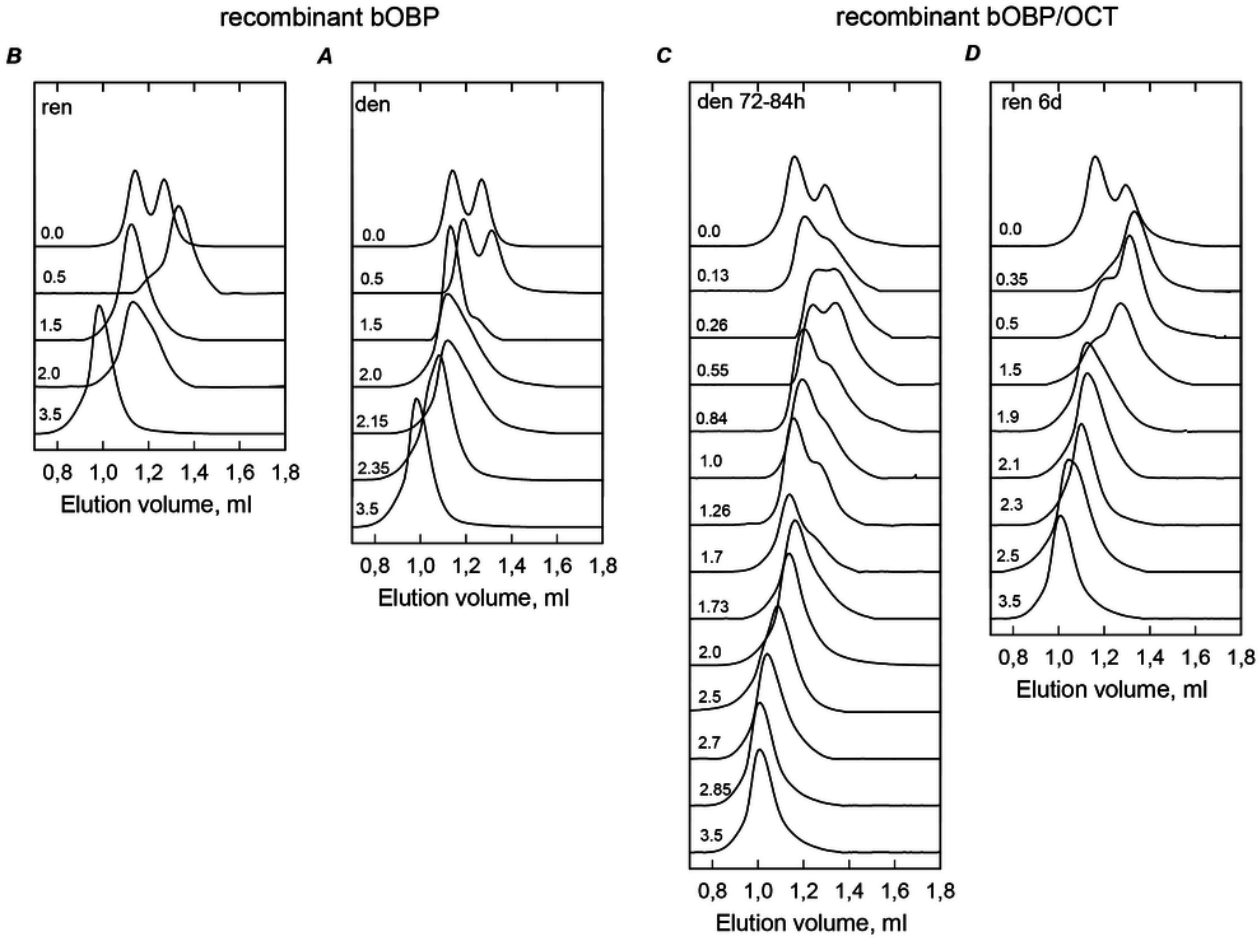

3

bOBP and bOBP/OCT conformational changes induced by GdnHCl.

A: changes in fluorescence intensity at 320 nm, λ_{ex}=297 nm; ***B***: changes in parameter *A*, λ_{ex}=297 nm; ***C***: changes in fluorescence anisotropy at the emission wavelength 365 nm, l_{ex}=297 nm; ***D***: changes in the ellipticity at 222 nm; ***E***: changes in the ANS fluorescence intensity at λ_{ex}=365 nm, λ_{em}=480 nm. The statistical errors for fluorescence measurements were assessed and were shown to fall within the range of 0.2 - 1 %. The measurements were preceded by incubating the protein in a solution with the appropriate GdnHCl concentration at 4 ºC for 24 (red circles) in the case of bOBP. The open symbols indicate unfolding, whereas the closed symbols represent refolding. While studying the folding of bOBP/OCT (squares), the solution of complex of the protein with its ligand were incubated in a solution with the appropriate GdnHCl concentration at 4 ºC for less than 24 h (open brown squares), up to 120 h (open pink squares) at the protein denaturation, and 1 h (closed brown squares) and 72 h – 30 days (closed pink squares) at the protein renaturation.

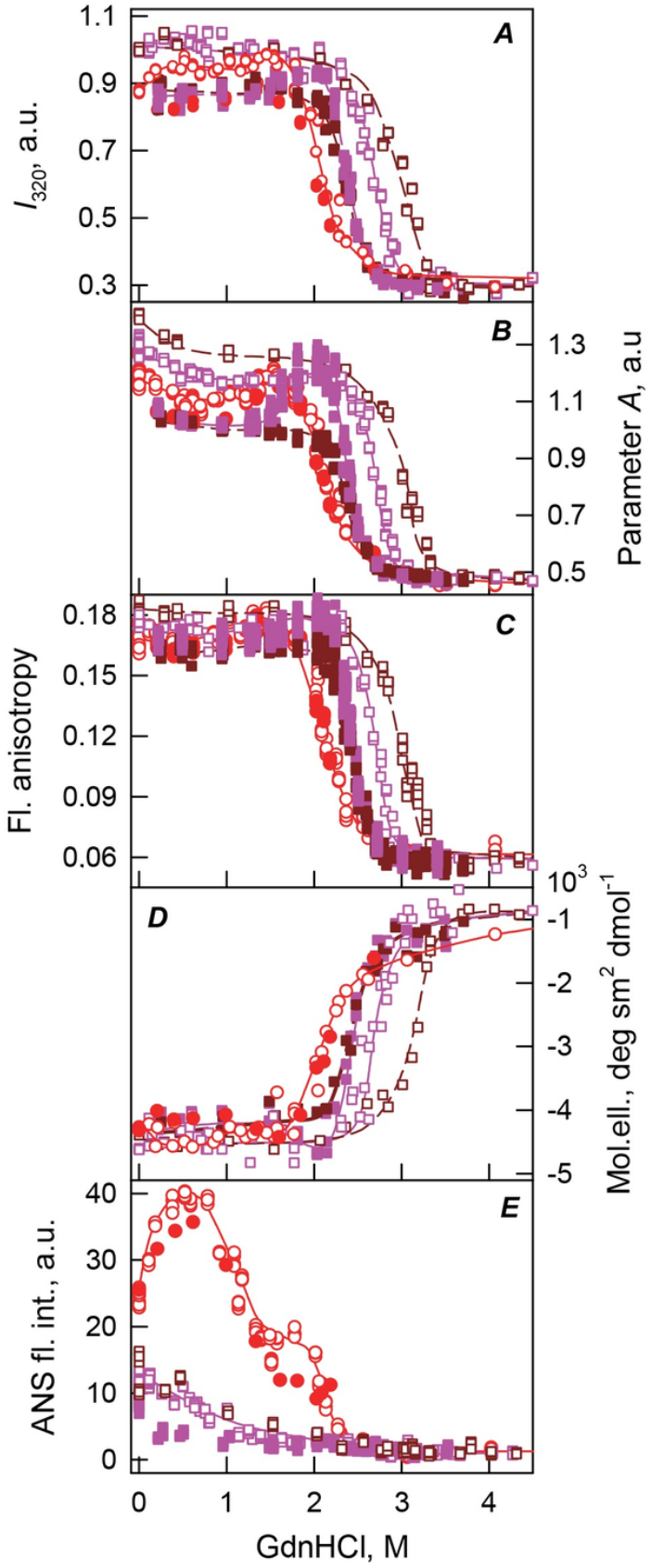
A
B
C
D
E
I_{320}, a.u.
Parameter A, a.u
Fl. anisotropy
Mol.ell., deg sm^2 dmol^{-1}
10^3
ANS fl. int., a.u.
GdnHCl, M

4

The changes of hydrodynamic dimensions of recombinant bOBP-Gly121+ (*A* and *B*) and its complex with ligand bOBP-Gly121+/OCT (*C* and *D*) in different structural states.

The elution profiles for bOBP-Gly121+ and bOBP-Gly121+/OCT were recorded during the protein denaturation (***A*** and ***C***) and renaturation from unfolded states (***B*** and ***D***) induced by GdnHCl. The elution profiles for bOBP-Gly121+ were measured after pre-incubation of the protein and the solution of GdnHCl in desired concentration for 24h (***A*** and ***B***), while in the case of bOBP-Gly121+/OCT the incubation time was extended to 72 – 84 h for denaturation (***C***) and 6 days for renaturation (***D***). The figures on the curves are the GdnHCl concentrations.

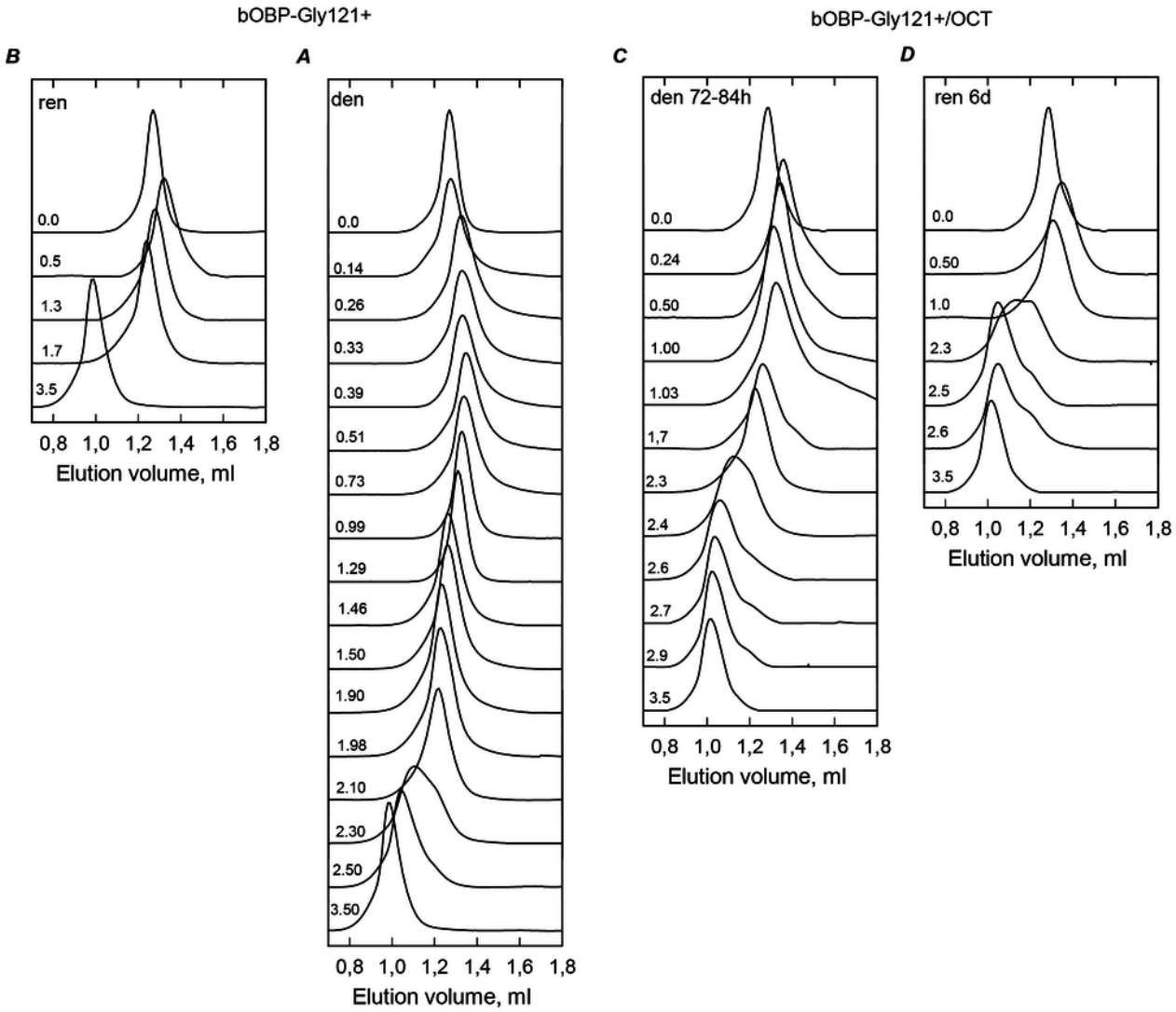
bOBP-Gly121+
bOBP-Gly121+/OCT
B
ren
0.0
0.5
1.3
1.7
3.5
0,8 1,0 1,2 1,4 1,6 1,8
Elution volume, ml
A
den
0.0
0.14
0.26
0.33
0.39
0.51
0.73
0.99
1.29
1.46
1.50
1.90
1.98
2.10
2.30
2.50
3.50
0,8 1,0 1,2 1,4 1,6 1,8
Elution volume, ml
C
den 72-84h
0.0
0.24
0.50
1.00
1.03
1,7
2.3
2.4
2.6
2.7
2.9
3.5
0,8 1,0 1,2 1,4 1,6 1,8
Elution volume, ml
D
ren 6d
0.0
0.50
1.0
2.3
2.5
2.6
3.5
0,8 1,0 1,2 1,4 1,6 1,8
Elution volume, ml

5

Figure 4. bOBP-Gly121+ and bOBP-Gly121+/OCT conformational changes induced by GdnHCl.

A: changes in fluorescence intensity at 320 nm, λ_{ex}=297 nm; ***B***: changes in parameter *A*, λ_{ex}=297 nm; ***C***: changes in fluorescence anisotropy at the emission wavelength 365 nm, l_{ex}=297 nm; ***D***: changes in the ellipticity at 222 nm; ***E***: changes in the ANS fluorescence intensity at λ_{ex}=365 nm, λ_{em}=480 nm. The measurements were preceded by incubating the protein in a solution with the appropriate GdnHCl concentration at 4 ºC for 24 (dark green circles) in the case of bOBP-Gly121+. The open symbols indicate unfolding, whereas the closed symbols represent refolding. While studying the folding of bOBP-Gly121+/OCT (squares), the solution of complex of the protein with its ligand were incubated in a solution with the appropriate GdnHCl concentration at 4 ºC for less than 24 h (open dark yellow squares), up to 72 h (open light green squares) at the protein denaturation, and 1 h (closed dark yellow squares) and 72 h (closed light green squares) at the protein renaturation.

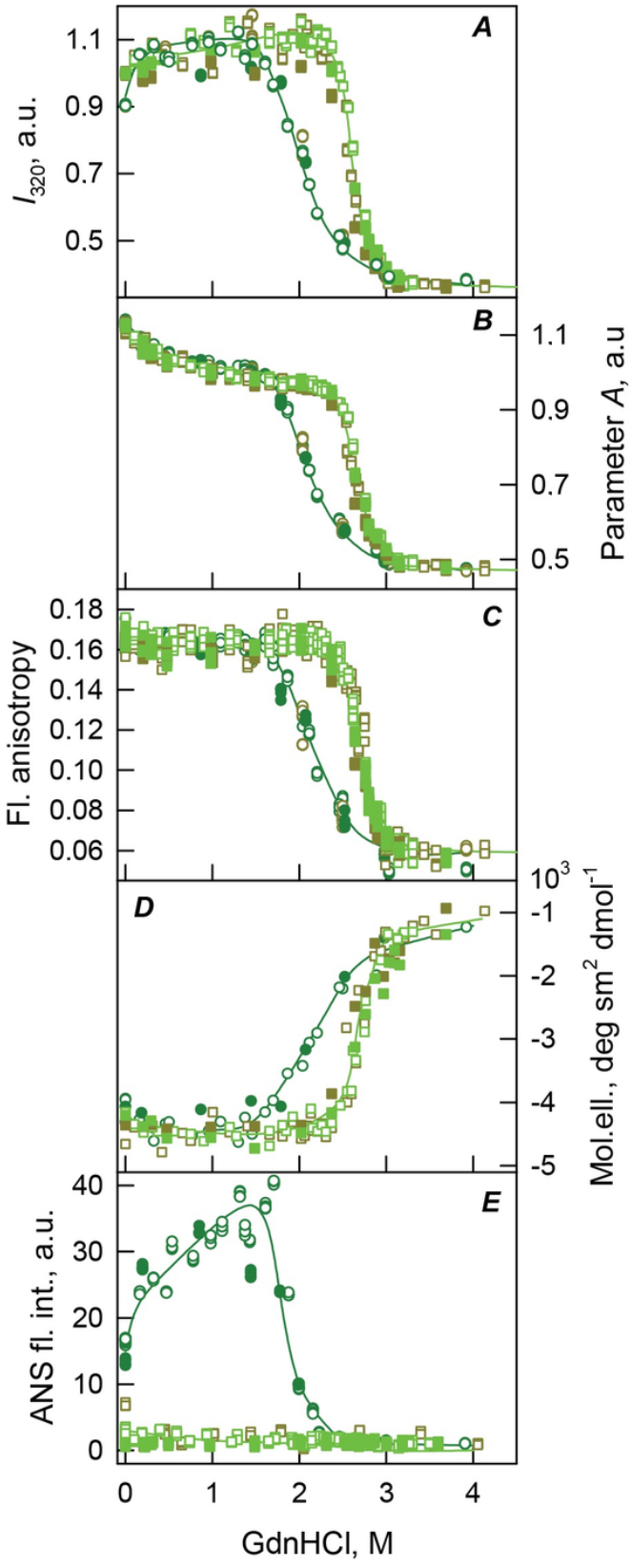
A
B
C
D
E
I_{320}, a.u.
Parameter A, a.u
Fl. anisotropy
Mol.ell., deg sm^2 dmol^{-1}
10^3
ANS fl. int., a.u.
GdnHCl, M

6

The changes of hydrodynamic dimensions of recombinant GCC-bOBP (*A* and *B*) and its complex with ligand GCC-bOBP/OCT (*C* and *D*) in different structural states.

The elution profiles for GCC-bOBP and GCC-bOBP/OCT were recorded during the protein denaturation (***A*** and ***C***) and renaturation from unfolded states (***B*** and ***D***) induced by GdnHCl. The elution profiles for GCC-bOBP were measured after pre-incubation of the protein and the solution of GdnHCl in desired concentration for 24h (***A*** and ***B***), while in the case of GCC-bOBP/OCT the incubation time was extended to 72 – 84 h for denaturation (***C***) and 6 days for renaturation (***D***). The figures on the curves are the GdnHCl concentrations.

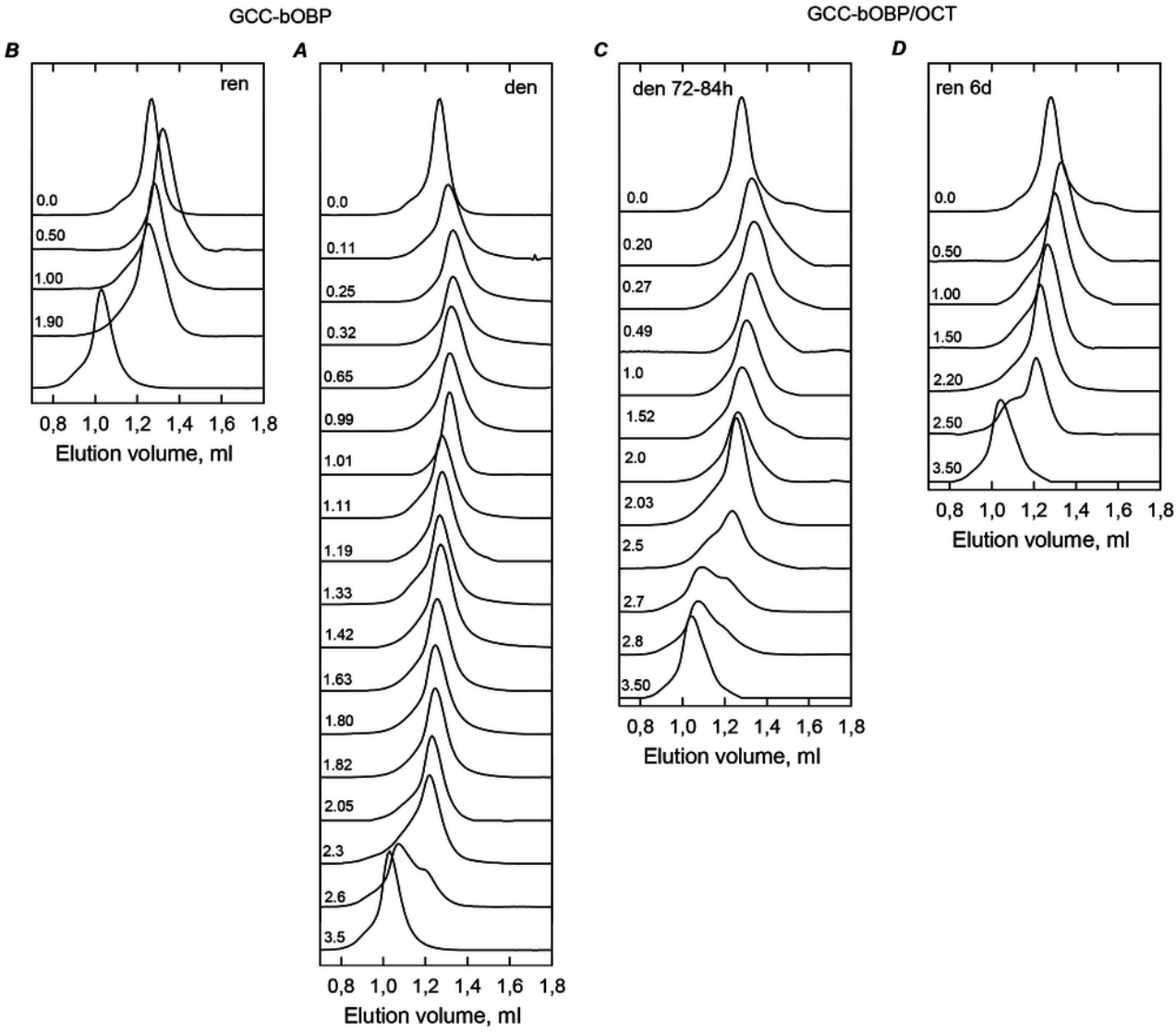
GCC-bOBP
GCC-bOBP/OCT
B
ren
0.0
0.50
1.00
1.90
0,8 1,0 1,2 1,4 1,6 1,8
Elution volume, ml
A
den
0.0
0.11
0.25
0.32
0.65
0.99
1.01
1.11
1.19
1.33
1.42
1.63
1.80
1.82
2.05
2.3
2.6
3.5
0,8 1,0 1,2 1,4 1,6 1,8
Elution volume, ml
C
den 72-84h
0.0
0.20
0.27
0.49
1.0
1.52
2.0
2.03
2.5
2.7
2.8
3.50
0,8 1,0 1,2 1,4 1,6 1,8
Elution volume, ml
D
ren 6d
0.0
0.50
1.00
1.50
2.20
2.50
3.50
0,8 1,0 1,2 1,4 1,6 1,8
Elution volume, ml

7

GCC-bOBP and GCC-bOBP/OCT conformational changes induced by GdnHCl.

A: changes in fluorescence intensity at 320 nm, λ_{ex}=297 nm; ***B***: changes in parameter *A*, λ_{ex}=297 nm; ***C***: changes in fluorescence anisotropy at the emission wavelength 365 nm, l_{ex}=297 nm; ***D***: changes in the ellipticity at 222 nm; ***E***: changes in the ANS fluorescence intensity at λ_{ex}=365 nm, λ_{em}=480 nm. The measurements were preceded by incubating the protein in a solution with the appropriate GdnHCl concentration at 4 ºC for 24 (blue circles) in the case of GCC-bOBP. The open symbols indicate unfolding, whereas the closed symbols represent refolding. While studying the folding of GCC-bOBP/OCT (squares), the solution of complex of the protein with its ligand were incubated in a solution with the appropriate GdnHCl concentration at 4 ºC for less than 24 h (open dark blue squares), up to 72 h (open light blue squares) at the protein denaturation, and 1 h (closed dark blue squares) and 72 h (closed light blue squares) at the protein renaturation.

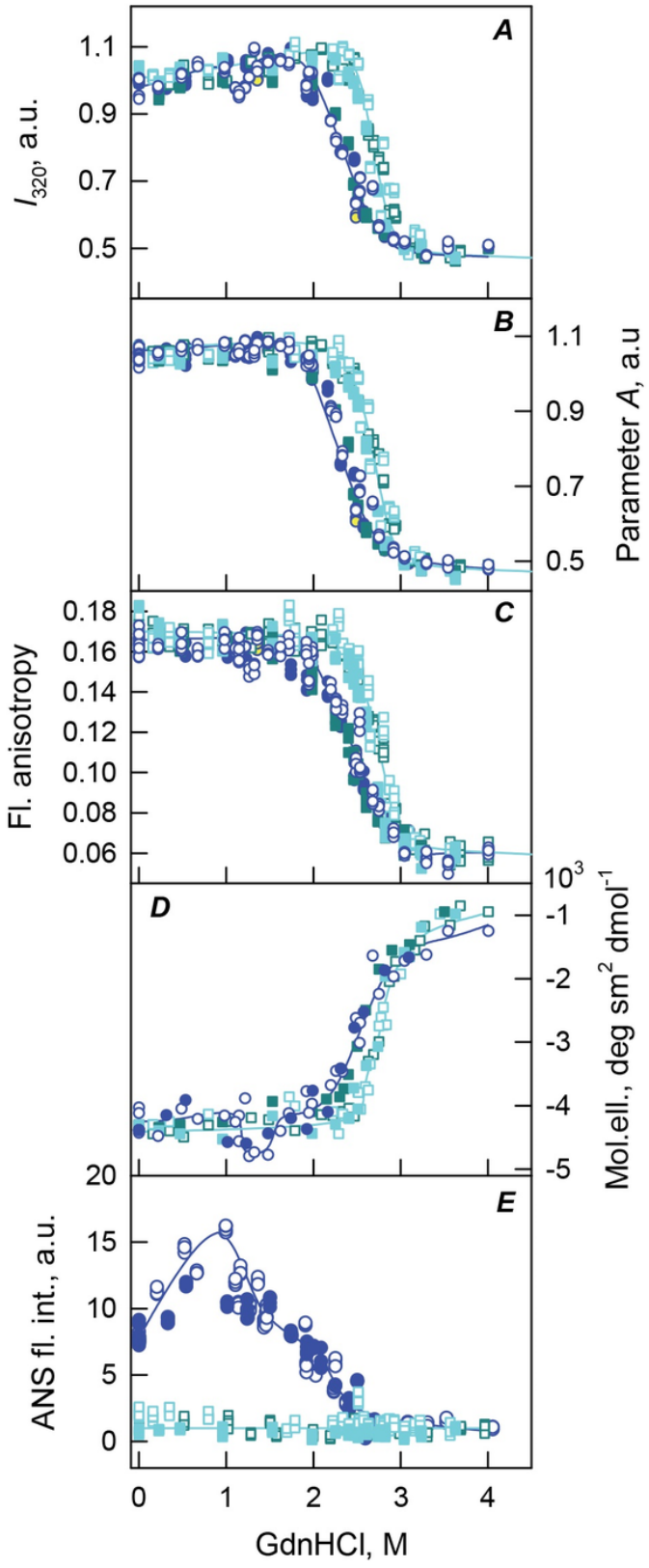
A
B
C
D
E
I_{320}, a.u.
Parameter A, a.u
Fl. anisotropy
Mol.ell., deg sm^2 dmol^{-1}
10^3
ANS fl. int., a.u.
GdnHCl, M